Strojnícky časopis – *Journal of* MECHANICAL ENGINEERING,
VOL 75 (2025), NO 1, 135 – 146

ANALYSIS OF CONICAL PART OF INTEGRALLY WOUND COMPOSITE PRESSURE VESSEL SUBJECTED TO INTERNAL PRESSURE AND TEMPERATURE LOADING

PADOVEC Zdeněk[1]

[1] *Czech Technical University in Prague, Faculty of Mechanical Engineering, Department of Mechanics, Biomechanics and Mechatronics, Technická 4, 160 00, Prague, Czech Republic, e – mail: zdenek.padovec@fs.cvut.cz*

Abstract: The presented article focuses on membrane solution of conical part from integrally wound conical pressure vessel. Wall of cone consist of three layers with (90/±ω0/90) symmetrical lay-up. Combination of netting theory and theory of orthotropic continuum was used for stress analysis. The cone was loaded by internal pressure and uniform temperature change. Obtained results for both loading cases were compared with the results from Finite Element Method (FEM) with achieving good agreement.

KEYWORDS: Conical pressure vessel, Filament winding, Stress analysis, Internal pressure, Temperature loading, FEM.

1 Introduction

Most of the composite pressure vessels manufactured by the means of filament winding consist of cylindrical part with end domes [1], [2]. In many practical cases it is necessary to use different shape than cylinder with domes –sphere which has the smallest surface area of all surfaces that enclose a given volume [3], toroid which is a promising for gaseous fuel tank design due to its space-saving and weight-reducing potential, its lack of structurally inefficient domed heads [4], [5] or cone shape which is widely used in the aerospace, aeronautic and in general industries as the shell of revolution either in curved panels or in conical frustum [6, 7, 8] and which was chosen for analysis.

Presented analysis presume that cone angle γ is so small that the shell can be made by applying the process used for cylindrical pressure vessels which consists of a helical angle-ply $\pm\omega_0$ geodesic layer forming the conical section and the domes of the vessel and hoop layers (ω=90°) reinforcing the conical section [9]. Also, membrane stress state was presumed. Theory of orthotropic continuum respectively classic lamination theory (CLT) and selected strength criteria can be used for obtaining stress/strain equations for given geometry [10, 11, 12, 13]. Conical part of the integrally wound pressure vessel was analyzed for the loading by internal pressure but also with the effect of uniform temperature field loading with the focus on cooling after the curing cycle which causes residual stresses in the construction [14, 15].

Composite cones can be also analyzed with FEM [16]. Obtained analytical results were compared with results from FE solution for given numerical example and both loading cases.

2 Materials and methods

2.1 Conical geometry of filament wound vessel

The presented article will deal with conical shell which is a part of integrally wound pressure vessel with domes (see Figure 1.). Defined boundaries are

$$\begin{aligned} s \le y \le l \\ a_U \le r \le a_{,L} \end{aligned} \tag{1}$$

where a_U and a_L are radii of upper/lower base of the cone, *y* is variable meridional coordinate with axial coordinate *z* and radial coordinate *r*.

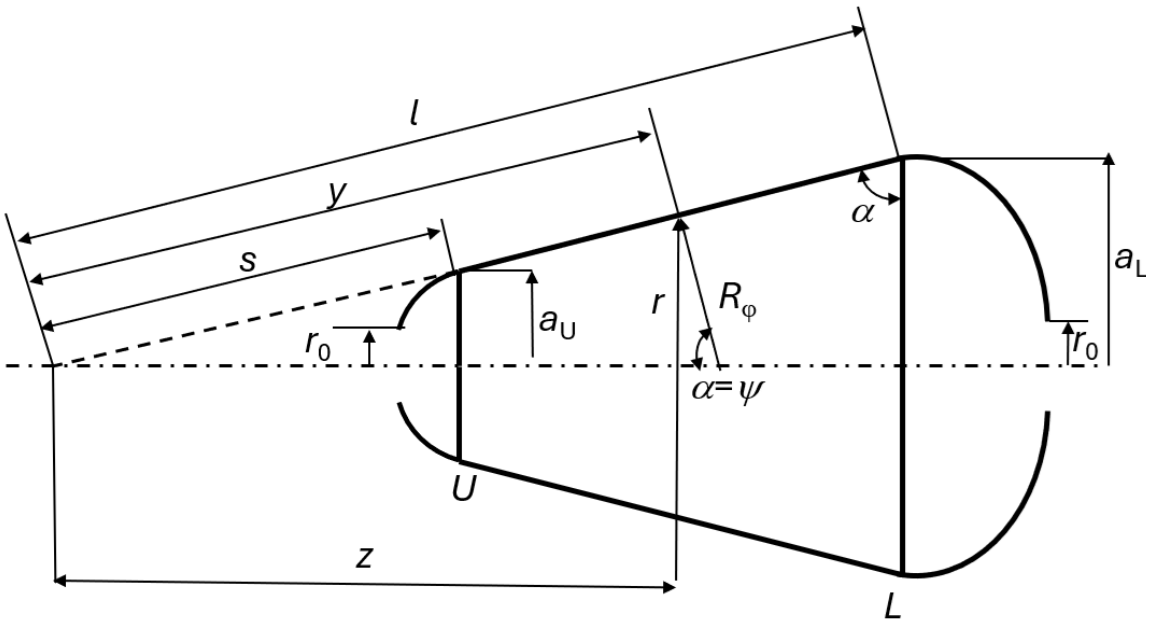

Fig. 1 Geometry of integrally wound conical pressure vessel

Even there is no meridian curvature $\left(\frac{1}{R_\psi} = 0\right)$ the second principal radius R_φ, wall thickness *h* and winding angle ω depend on axial (meridional) coordinate *z* (*y*). The radius of polar openings r_0 has same dimensions for analyzed case. α is angle between cone surface line and bases and it is the same as ψ which is angle between normal and shell midplane.

The conical part of integrally wound pressure vessel consists of three-layered wall with ($90/\pm\omega_0/90$) lay-up which as same as in the case of wound cylinder. Winding angle ω should respect geodesic condition

$$\sin\omega_{0U} = \frac{r_0}{a_U}, \text{ and} \sin\omega_{0L} = \frac{r_0}{a_L}, \tag{2}$$

so angle of the balanced layer is

$$\omega_{0U} \ge \omega_0 \ge \omega_{0L}. \tag{3}$$

Cone angle can be maximum

$$\gamma = 90 - \alpha = \tan^{-1} f = \tan^{-1} 0{,}2 = 11.3°, \tag{4}$$

where *f* is frictional coefficient, and it is equal to 0.2 for wet winding because parallel circles of the conical surface are not geodesic lines [9].

For each shell with double curvature is typical change in the wall thickness caused by the winding of a tape of a constant width on a different radius *r*. The wall thickness of the balanced layer can be computed as [17].

$$h_o = h_{oL} \frac{a_L}{r} \frac{\cos\omega_{oL}}{\cos\omega_o}, \tag{5}$$

where h_{0L} is the thickness on the lower base radius. Wall thickness of hoop layers h_1 is constant if the speed of the delivery eye is also constant [9]. Thickness of three-layered wall is

$$h = 2h_1 + h_0. \tag{6}$$

Optimal wall thickness which respects geodesical and isotensoidal conditions according to netting theory [16] can be achieved only on lower base radius

$$\frac{2h_1}{h_0} = 3\cos^2\omega_{0L} - 1. \tag{7}$$

2.2 Thermoelastic properties of three-layered wound wall

Let´s consider a glass/epoxy system with thermoelastic and strength properties (according to the coordinate system in Figure 2) given in Tables 1 and 2 [2].

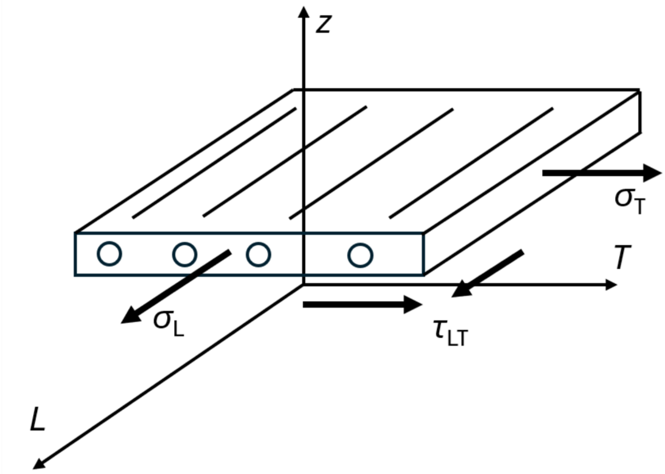

Fig. 2 Coordinate system of material orthotropy

Table 1. Thermoelastic properties of considered glass/epoxy material system

Material	E_L [MPa]	E_T [MPa]	G_{LT} [MPa]	υ_{LT} [MPa]	α_L[K^{-1}]	α_T[K^{-1}]
Glass/epoxy	48 000	17 600	8 000	0.25	$6.5 \cdot 10^{-6}$	$16.3 \cdot 10^{-6}$

Table 2. Strength properties of considered glass/epoxy material system

Material	F_{Lt} [MPa]	F_{Lc} [MPa]	F_{Tt} [MPa]	F_{Tc} [MPa]	F_{LT} [MPa]
Glass/epoxy	1 200	600	45	145	65

where *L* stands for longitudinal direction, *T* for transversal direction, *t* for tension, and *c* for compression.

Analyzed three-layered wound wall has (90/±ω_0/90) lay-up. Symmetrical lay-up of balanced layers excludes shear deformation due to rotationally symmetrical load so elements of stiffness matrix Q_{ij} for three layered wall $Q_{16} = Q_{26} = 0$.

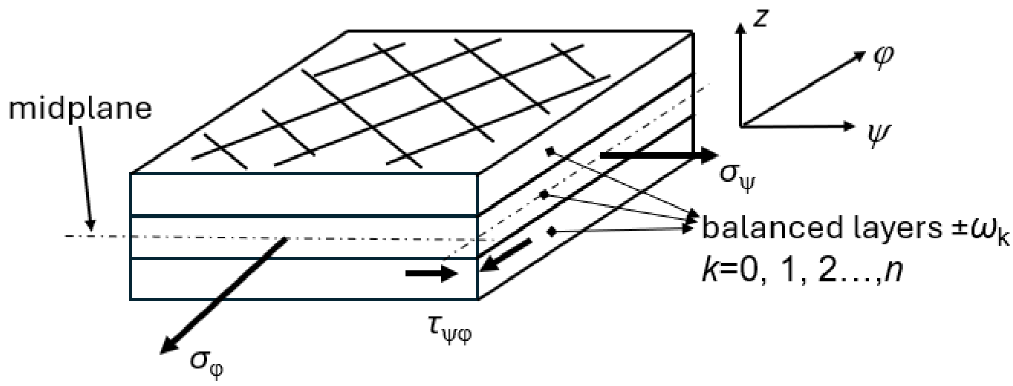

Fig. 3 Geometry of three-layered wall

Duhamel-Neumann law for three-layered wall (Figure 3) can be written

$$\begin{bmatrix}\sigma_\psi\\ \sigma_\varphi\\ \tau_{\psi\varphi}\end{bmatrix} = \begin{bmatrix}Q_{11} & Q_{12} & 0\\ Q_{21} & Q_{22} & 0\\ 0 & 0 & Q_{66}\end{bmatrix}\left\{\begin{bmatrix}\varepsilon_\psi\\ \varepsilon_\varphi\\ \gamma_{\psi\varphi}\end{bmatrix} - \Delta T\begin{bmatrix}\alpha_\psi\\ \alpha_\varphi\\ 0\end{bmatrix}\right\}, \tag{8}$$

where $Q_{ij} = \sum_k \frac{h_k}{h}\overline{Q_{ij}^k}$. $\overline{Q_{ij}^k}$ is stiffness matrix for balanced layer, where k=0 for layers with winding angle $\pm\omega_0$ and k=1 for hoop layers with winding angle 90° (elements $\overline{Q_{16}} = \overline{Q_{26}} = 0$). α_ψ and α_φ are coefficients of thermal expansion (CTE´s) for three-layered wall. (see [19] for details).

Elastic properties for whole three-layered wall can be calculated as (see [20] for details)

$$E_\psi = \frac{1}{h}\left(A_{11} - \frac{A_{12}^2}{A_{22}}\right), E_\varphi = \frac{1}{h}\left(A_{22} - \frac{A_{12}^2}{A_{11}}\right) \ldots \tag{9}$$

where A_{ij} are elements of membrane stiffness matrix which can be computed for three-layered wall as

$$A_{ij} = \sum_k \overline{A_{ij}^k} = \sum_k \overline{Q_{ij}^k} h_k \, . \tag{10}$$

CTE´s for three-layered wall are

$$\begin{aligned}\alpha_\psi &= \frac{A_{22}\left(\sum \overline{{}^kA_{11}\,{}^k\alpha_\psi} + \sum \overline{{}^kA_{12}\,{}^k\alpha_\varphi}\right) - A_{12}\left(\sum \overline{{}^kA_{12}\,{}^k\alpha_\psi} + \sum \overline{{}^kA_{22}\,{}^k\alpha_\varphi}\right)}{A_{11}A_{22} - A_{12}^2},\\ \alpha_\varphi &= \frac{A_{11}\left(\sum \overline{{}^kA_{22}\,{}^k\alpha_\varphi} + \sum \overline{{}^kA_{12}\,{}^k\alpha_\psi}\right) - A_{12}\left(\sum \overline{{}^kA_{12}\,{}^k\alpha_\varphi} + \sum \overline{{}^kA_{11}\,{}^k\alpha_\psi}\right)}{A_{11}A_{22} - A_{12}^2},\end{aligned} \tag{11}$$

where $\overline{{}^k\alpha_\psi}$ and $\overline{{}^k\alpha_\varphi}$ are CTE´s for balanced layer (see [18] for details).

2.3 Loading by internal pressure

Loading by internal pressure (Figure 4) causes strains in the composite wall which can be computed as

$$\begin{bmatrix}\varepsilon_\psi\\ \varepsilon_\varphi\\ \gamma_{\psi\varphi}\end{bmatrix} = \begin{bmatrix}a_{11} & a_{12} & 0\\ a_{21} & a_{22} & 0\\ 0 & 0 & a_{66}\end{bmatrix}\begin{bmatrix}N_\psi\\ N_\varphi\\ 0\end{bmatrix}, \tag{12}$$

where $a_{ij} = {A_{ij}}^{-1}$.

Forces from (12) can be computed like

$$N_\psi = \frac{pr}{2\sin\alpha}, N_\varphi = \frac{pr}{\sin\alpha}, N_{\psi\varphi} = 0, \tag{13}$$

where p is internal pressure.

Stresses in each layer can be computed from

$$\begin{bmatrix}\sigma_\psi\\ \sigma_\varphi\\ \tau_{\psi\varphi}\end{bmatrix}_k = \begin{bmatrix}Q_{11} & Q_{12} & Q_{16}\\ Q_{21} & Q_{22} & Q_{26}\\ Q_{16} & Q_{26} & Q_{66}\end{bmatrix}_k \begin{bmatrix}\varepsilon_\psi\\ \varepsilon_\varphi\\ 0\end{bmatrix}. \tag{14}$$

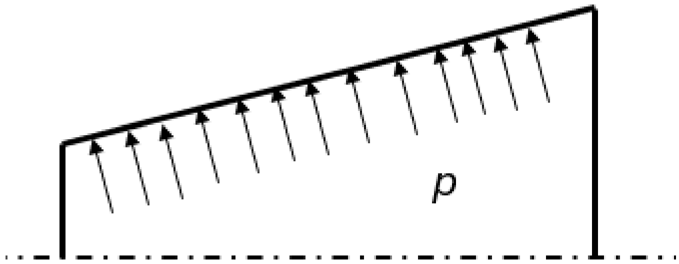

Fig. 4 Conical part of pressure vessel loaded by internal pressure

2.4 Loading by uniform temperature field

With respect to the assumption of thin-walled construction ($h \ll a$), the uniform distribution of temperature change ΔT which is constant throughout the wall thickness induces a constant strain distribution throughout the wall thickness. Stresses in the three-layered wall can be computed from

$$\begin{bmatrix} \sigma_\psi \\ \sigma_\varphi \\ \tau_{\psi\varphi} \end{bmatrix}_k = \begin{bmatrix} \overline{Q_{11}} & \overline{Q_{12}} & 0 \\ \overline{Q_{12}} & \overline{Q_{22}} & 0 \\ 0 & 0 & \overline{Q_{66}} \end{bmatrix}_k \begin{bmatrix} \alpha_\psi - \overline{\alpha_\psi} \\ \alpha_\varphi - \overline{\alpha_\varphi} \\ 0 \end{bmatrix}_k \Delta T. \qquad (15)$$

Shear stress in orthotropic monolayer can be written as

$$^k\tau_{\psi\varphi} = {}^kG_{\psi\varphi}\left(- {}^kS_{61}\,{}^k\sigma_\psi - {}^kS_{62}\,{}^k\sigma_\varphi - \alpha_{\psi\varphi}\Delta T\right), \qquad (16)$$

where $^kG_{\psi\varphi}$ is shear modulus of helical or hoop layer (k=0, 1), $^kS_{61}$ and $^kS_{62}$ are elements of compliance matrix for oriented monolayer and $\alpha_{\psi\varphi}$ is shear CTE for oriented monolayer (see [20] for details).

2.5 Application of stress criterion

For both loading cases described in Sections 2.3 and 2.4 is necessary to transform stresses from a global coordinate system to a local system of material orthotropy (see Figure 5).

$$\begin{bmatrix} \sigma_L \\ \sigma_T \\ \tau_{LT} \end{bmatrix}_k = \begin{bmatrix} \cos^2\omega & \sin^2\omega & 2\cos\omega\sin\omega \\ \sin^2\omega & \cos^2\omega & -2\cos\omega\sin\omega \\ -\cos\omega\sin\omega & \cos\omega\sin\omega & \cos^2\omega - \sin^2\omega \end{bmatrix}_k \begin{bmatrix} \sigma_\psi \\ \sigma_\varphi \\ \tau_{\psi\varphi} \end{bmatrix}_k . \qquad (17)$$

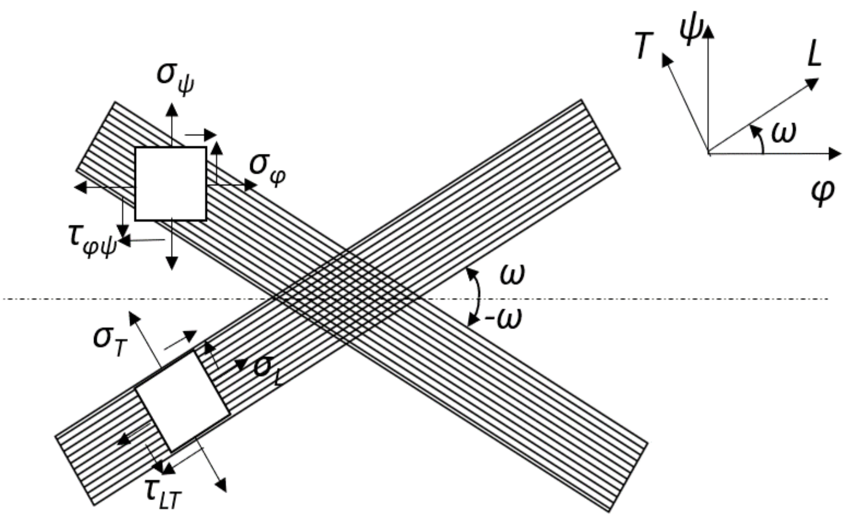

Fig. 5 Stress transformation [21]

Stresses, computed from (17) are used as input for the calculation of the failure index from the selected strength criterion. The maximum stress criterion was chosen (see [12] for example) and it states that failure occurs when at least one of the stresses in the material coordinates exceeds the corresponding experimental strength value. This can be expressed as

$$\begin{aligned} -F_{Lc} &< \sigma_L < F_{Lt}, \\ -F_{Tc} &< \sigma_T < F_{Tt}, \\ -F_{LT} &< \sigma_{LT} < F_{LT}, \end{aligned} \tag{18}$$

2.5 FE analysis

FE analysis was done using commercial software Abaqus. The geometry of the cone was cut with the use of parallels so the change in wall thickness and the change in winding angle can be affected. S4R shell elements were used for discretization. Size of the elements was chosen after performing mesh sensitivity test. The conical part of the vessel was joint with hemispherical domes to close the vessel. Domes were not part of the performed analysis. FE model can be seen in Figure 6. The result from the FE analysis for both loading cases (internal pressure and uniform temperature field) is the failure index according to the maximum stress criterion.

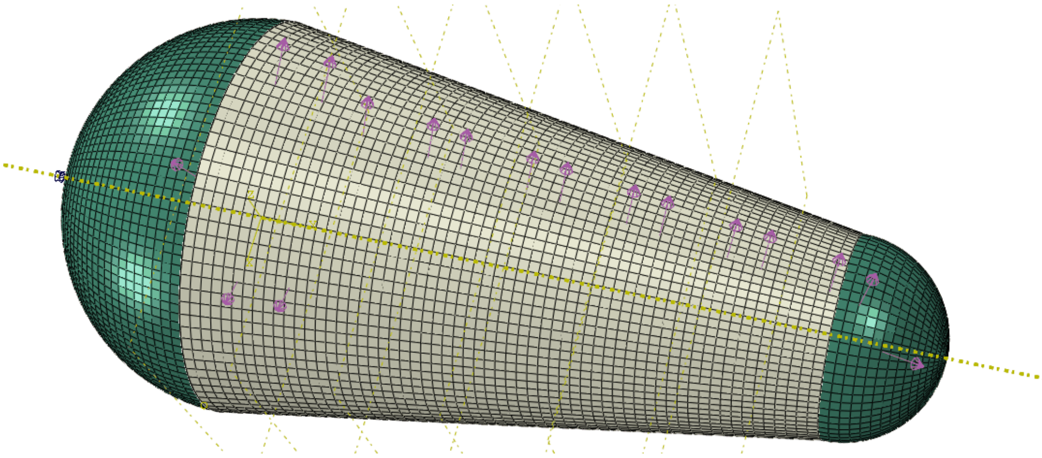

Fig. 6 Conical part of pressure vessel loaded by internal pressure

3 Results and discussion

3.1 Numerical example

The numerical example was computed for conus with $a_U = 100$ mm, $a_L = 200$ mm. Length of conical part of the vessel is 600 mm. Combination of this dimensions leads to the cone angle γ=9.46° and α=80.54°. The radius of both polar openings is r_0 = 50 mm. Thickness of balanced layer on lower base h_0 = 1 mm. Thickness of hoop layer calculated according to (7) leads to h_1 = 0.91 mm. Internal pressure is p = 1 MPa. The analyzed conical part was cooled from 120°C to 20° which corresponds to cooling after the curing cycle of typical epoxy resin. Also, cooling is more dangerous because σ_T has a tensile character for this material system. Failure index according to (18) was computed for both loading cases analytically and compared with results obtained by FEM. The comparison of the results is plotted in Figures 10 and 11.

Figure 10 depicts the relationship between the winding angle and position on the meridian. Winding angle is changing continuously from maximal value on upper base a_U radius to minimal value on lower base radius a_L From the last part of Figure 7 can be stated that minimal thickness is on the lower base radius and maximal on the upper base radius.

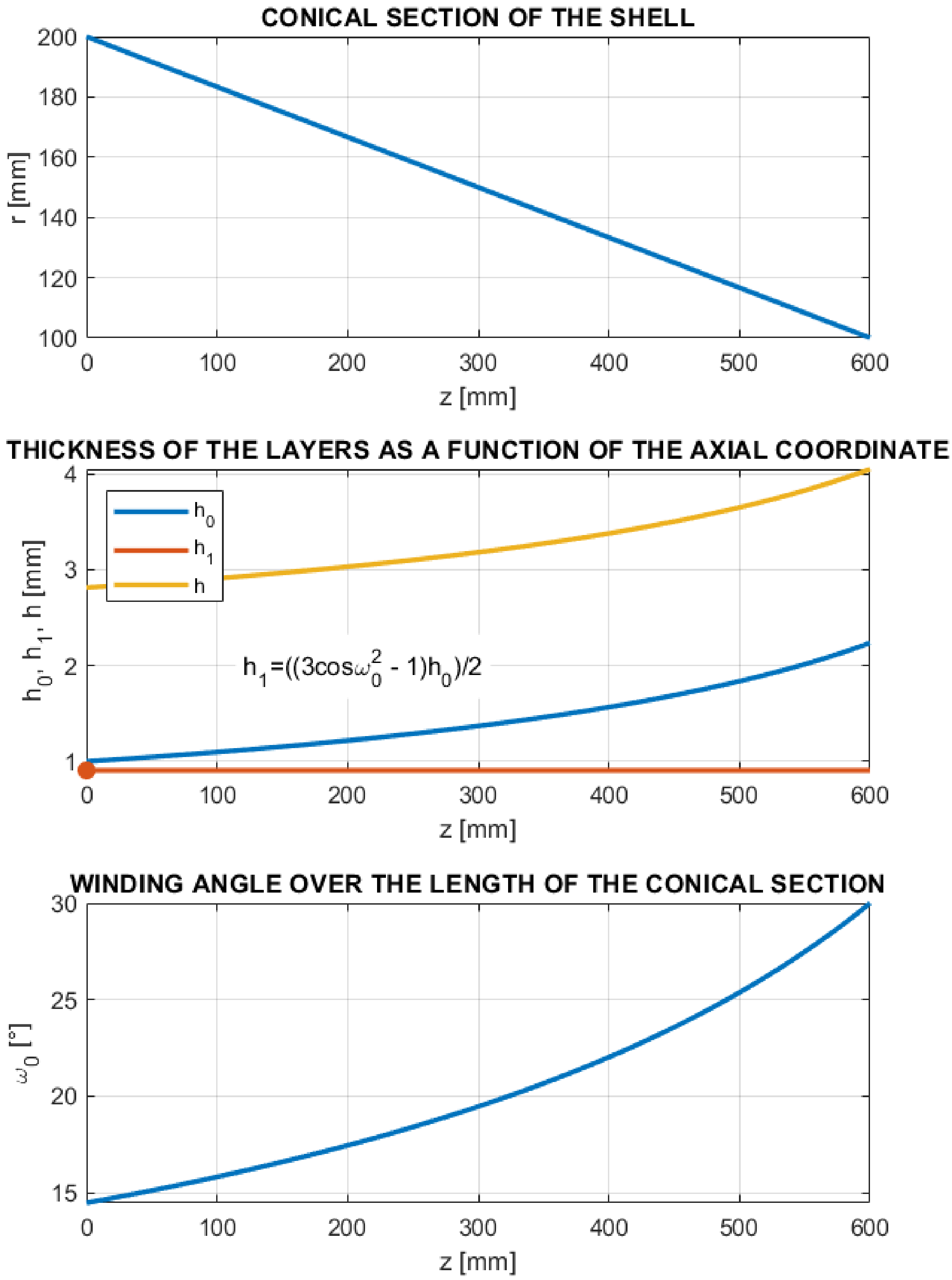

Fig. 7 Meridian of conical part, thickness of the layers and change in winding angle along meridional coordinate

Stresses from internal pressure in a global coordinate system calculated with the use of (12 - 14) can be normalized with axial stress on the lower dome equator. Stresses from temperature calculated with the use of (15) and (16) can be normalized with the use of ΔT.

$$\sigma_{sr} = \sigma_{\psi L} = \frac{pa_L}{2h_{0L}\sin\alpha}. \qquad (19)$$

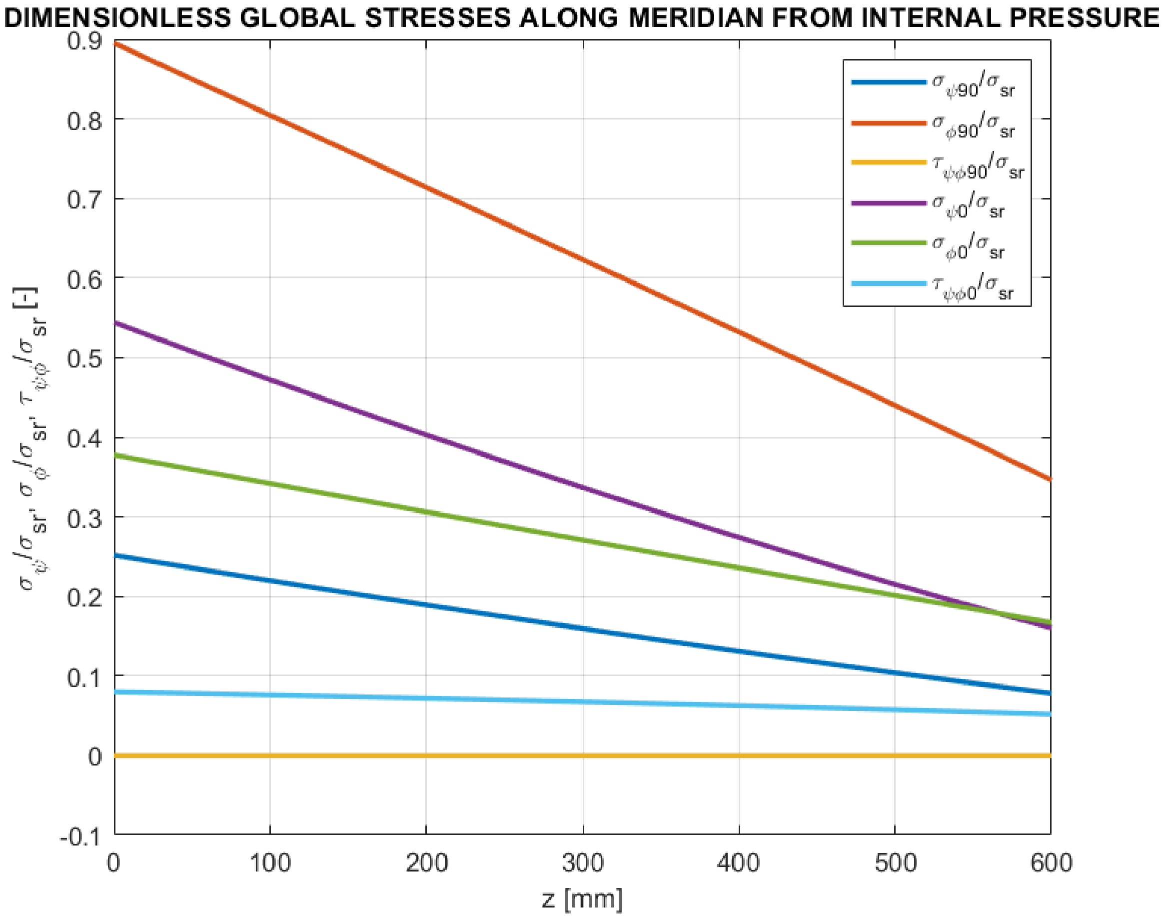

Fig. 8. Dimensionless global stresses from internal pressure

Dimensionless global stresses from internal pressure can be seen in Figure 8. Maximum values of normal and shear stresses (plotted for the positive value of winding angle + ω) for both helical and hoop windings are on the lower base of the cone where isotensoidal condition is applied. Shear stress for the negative value of winding angle -ω has the same value but the opposite sign. From Figure 8 is also evident that the upper part of the cone is underloaded because of thicker wall in this area.

Dimensionless global stresses from temperature change can be seen in Figure 9. Maximum values of tangential normal and shear stresses (plotted for the positive value of winding angle + ω) for both helical and hoop windings are on the lower base of the cone where isotensoidal condition is applied. For helical windings axial normal stresses maximum values (in absolute value) are also on the lower base of the cone. For hoop windings axial normal stresses maximum values are on upper base of the come. Shear stress for the negative value of winding angle -ω has the same value but the opposite sign.

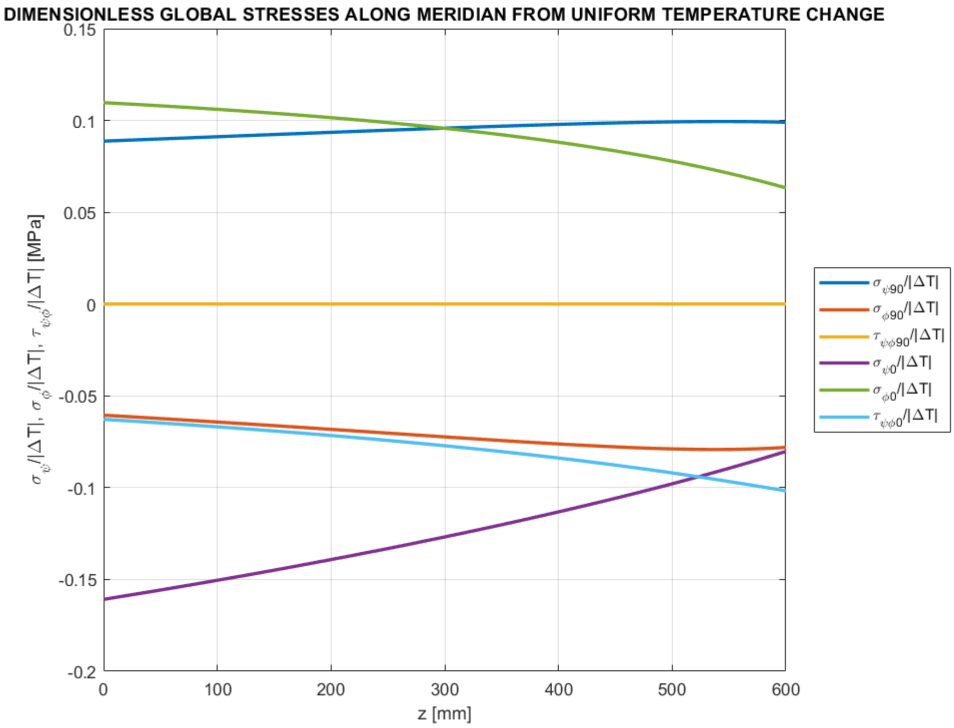

Fig. 9. Dimensionless global stresses from temperature change

These global stresses are transformed according to (17) and failure criterion (18) was used for failure index evaluation.

From the figures can be seen that the case of internal pressure loading (Figure 10) is maximum failure index on the lower base of the cone and minimal on the upper one. For the case of uniform cooling (Figure 11) the results are the same but the differences between lower and upper base of the cone are not as big as in case of internal pressure.

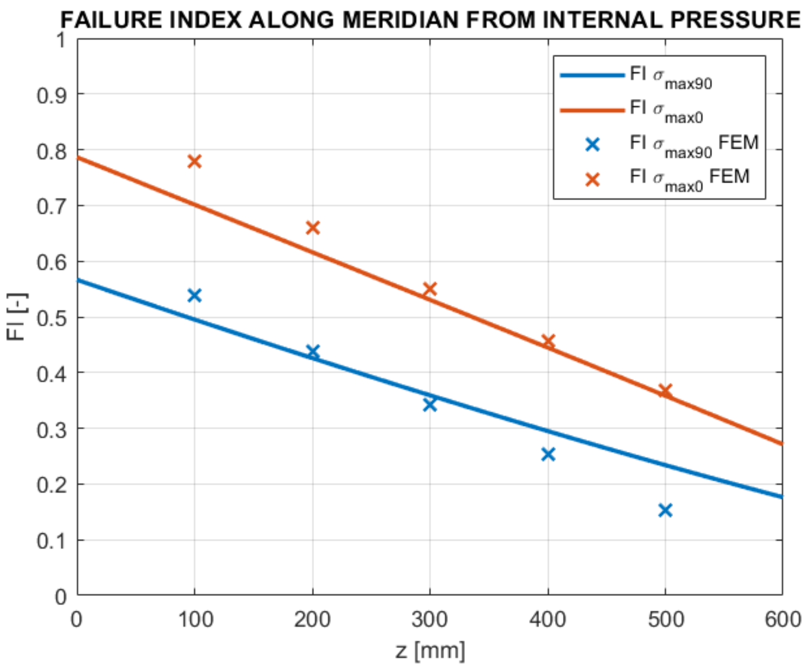

Fig. 10. Comparison of failure index for internal pressure load obtained analytically and numerically

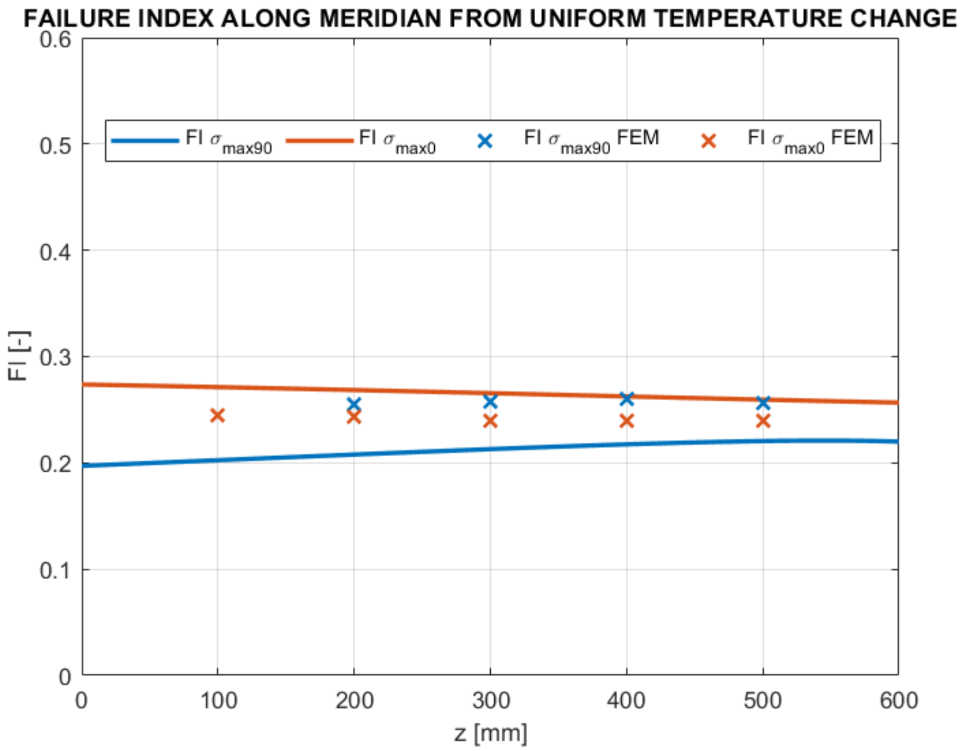

Fig. 11. Comparison of failure index for uniform temperature field obtained analytically and numerically

If the solution for the lower base of the cone, where the optimal wall thickness can be achieved, is compared with solution for cylinder [22] manufactured from the same material system with the same wall thicknesses loaded with the same pressure we obtain almost the same results (because of small value of the cone angle) which prove the correctness of presented solution. Global stresses in hoop and helical layers caused by internal pressure for both solutions are presented in Table 3.

Table 3. Comparison of global stresses caused by internal pressure for cone´s lower base and cylinder

	HOOP LAYERS			**HELICAL LAYERS**		
Stress	σ_ψ [MPa]	σ_φ [MPa]	$\tau_{\psi\varphi}$ [MPa]	σ_ψ [MPa]	σ_φ [MPa]	$\tau_{\psi\varphi}$ [MPa]
Cone – lower base	25.50	90.78	0	55.17	38.28	8.13
Cylinder	25.35	90.20	0	54.87	37.99	7.99

CONCLUSION

The analytical and numerical analysis of integrally wound conical pressure vessel with focus on conical part analysis was conducted for selected material system and numerical values. Analytical and numerical solution of failure index along the meridian was done for internal pressure load and uniform cooling with achieving good agreement. If the results from Figures 10 and 11 were superimposed together failure index reach a maximum value of around about 1.1 (in the lower base area). That means that temperature influence on resulting stresses has a nonnegligible effect and it should be an indisputable part of the pressure vessel analysis.

Future work will focus on joint of conical part of the vessel with selected domes and influence of membrane stress state violation in these areas on resulting failure index and possible optimization of the dome shape.

Acknowledgements

This study received support from the Grant Agency of the Czech Technical University in Prague, under grant No. SGS24/123/OHK2/3T/12.

REFERENCES

[1] Azeem, M., et al. "Application of Filament Winding Technology in Composite Pressure Vessels and Challenges: A Review", Journal of Energy Storage, 49, pp. 1 – 22, **2022**. DOI: 10.1016/j.est.2021.103468

[2] Liang, C. C., et al. "Optimum design of dome contour for filament-wound composite pressure vessels based on a shape factor", Composite Structures 58 (4), pp. 469 – 482, **2002**. DOI: 10.1016/S0263-8223(02)00136-8

[3] Zu, L., et al. "Design of filament-wound spherical pressure vessels based on non-geodesic trajectories", Composite Structures 218, pp. 71 – 78, **2019**. DOI: 10.1016/j.compstruct.2019.03.045

[4] Fowler, C. P., et. al. "A review of toroidal composite pressure vessel optimisation and damage tolerant design for high pressure gaseous fuel storage", International Journal of Hydrogen Energy 41 (47), pp. 22067 – 22089, **2016**. DOI: 10.1016/j.ijhydene.2016 .10.039

[5] Vick, J. M., et. al. "Finite Element Study on the Optimization of an Orthotropic Composite Toroidal Shell", Journal of Pressure Vessel Technology, Transactions of the ASME 134 (5), 051201, **2012**. DOI: 10.1115/1.4005873

[6] Pinto Correira, I. F., et al. "Analysis of laminated conical shell structures using higher order models", Composite Structures 62 (3-4), pp. 383 – 390, **2003**. DOI: 10.1016/j.compstruct.2003.09.009

[7] Jančo, R. "Stress Analysis of Pressing Joint of Two Coincal Pipes", Strojnícký časopis – Journal of Mechanical Engineering 73(1), pp. 117 – 124, **2023**. DOI: 10.2478/scjme-2023-0009

[8] Jančo, R. "Stress Analysis of Pressing Joint of Two Coincal Pipes – Part 2", Strojnícký časopis – Journal of Mechanical Engineering 74(2), pp. 43 – 48, **2024**. DOI: 10.2478/scjme-2024-0024

[9] Vasiliev, V. V. "Composite Pressure Vessels: Design, Analysis, and Manufacturing", Bull Ridge Publishing, Blacksburg, Virginia, USA**, 2009**.

[10] Chawla, K. K. "Composite Materials – Science and Engineering", 4th edition. Springer Nature Switzerland, Cham, Germany, **2019**.

[11] Barbero, E. J. "Introduction to Composite Material Design Second Edition", CRC Press, Boca Raton, Florida, USA, **2011**.

[12] Sharma, S. "Composite Materials - Mechanics, Manufacturing and Modeling", CRC Press, Boca Raton, Florida, USA, **2021**.

[13] Vinson, J. R. "The Behavior of Shells Composed of Isotropic and Composite Materials", Springer Science + Business Media, Dordrecht, Netherlands, **2013**.

[14] Liu, C., et. al. "Design optimization for filament wound cylindrical composite internal pressure vessels considering process-induced residual stresses", Composite Structures 235, 111755, **2020**. DOI: 10.1016/j.compstruct.2019.111755

[15] Maleki, S., et. al. "Non-linear analysis of fiber-reinforced open conical shell panels considering variation of thickness and fiber orientation under thermo-mechanical loadings", Composites Part B: Engineering 52, pp. 245-261, **2013**. DOI: j.compositesb.2013.04.026

[16] Shiravand, A., et. al. "Hybrid metal-composite conical tubes for energy absorption; theoretical development and numerical simulation", Thin-Walled Structures 145, 106442, **2019**. DOI: 10.1016/j.tws.2019.106442.

[17] Hofeditz, J. T. "Structural Design Considerations for Fibrous Glass Pressure Vessels", Modern Plastics, 41, pp. 127 – 145, **1964**.

[18] Gay, D. "Composite materials: Design and Applications", CRC Press, Boca Raton, Florida, USA, **2002**.

[19] Vondráček, D., et. al. "Analysis of Thermoelastic Stresses in Filament Wound Composite Pressure Vessels Using Evolutionary Deep Learning and Many-objective Optimisation", Philosophical Magazine Letters 105 (1), 2476499, **2025**. DOI: 10.1080/09500839.2025.2476499

[20] Ehrenstein, G. W. "Polymeric Materials Structure – Properties – Applications", Carl Hanser Verlag GmbH& Co. KG, Munich, Germany, N., **2001**.

[21] Padovec, Z., et. al. "The analytical and numerical stress analysis of various domes for composite pressure vessels", Applied and Computational Mechanics 16(2), pp. 151 – 166, **2022**. DOI: 10.24132/acm.2022.781

[22] Padovec, Z, et. al. "Stress Analysis in Filament Wounded Composite Pressure Vessels", In: PROCEEDINGS OF COMPUTATIONAL MECHANICS **2022**. Computational Mechanics 2022, Srní, 2022-11-07/2022-11-09. Plzeň: University of West Bohemia, pp. 103 – 106, **2022**. ISBN 978-80-261-1116-0. Available from: https://compmech.kme.zcu.cz/download/proceedings/CM2022_Conference_Proceedings.pdf